RECENT DEVELOPMENTS IN SHOCK ISOLATION FOR MARS MISSION INSIGHT

B. T. Kletz, J. Melcher,
Deutsches Zentrum für Luft- und Raumfahrt, Lilienthalplatz 7, 38108 Braunschweig, Germany

Abstract

The InSight mission was postponed from 2016 to launch in May 2018 when it will investigate the composition of planet Mars. DLRs HP³ instrument - a heat flow probe that hammers itself 5 meters into the Martian soil – is a key element of this mission. Though it was ready to launch in 2016 the delay has been used to further improve the instrument.

The implications for the shock isolation system that is integrated into this probe are highlighted within this paper. Its task is to protect the sensors within the probe from the very high shock accelerations that are generated during hammering. The isolation system reduces the shock loads that the sensors encounter in the updated probe design by factor 31.

1. INTRODUCTION

The 2018 InSight mission (Interior Exploration using Seismic Investigations, Geodesy and Heat Transport) is all about studying the deep interior of planet Mars. It will contribute valuable information in how the terrestrial planets in our solar system evolved. The mission is jointly operated by NASA, DLR and CNES and was originally planned to launch in 2016 [1].

DLR is responsible for the HP³ instrument (Heat Flow and Physical Properties Package) one of the major scientific payloads (cf. FIGURE 1) [1]. This instrument is based on a heat flow probe – the „mole“ – that will hammer itself 5 meters into the soil. Its main task is to determine the heat flow of the ground at multiple soil depths. The probe is therefore equipped with heaters and multiple temperature sensors along a tether that is pulled out of a support structure into the soil.

To determine the heat flow, the depth of the probe within the ground must be precisely known. This information is gained by measuring the pulled out length of the tether and by determining the tilt of the probe inside the Martian soil. To do so, two very sensitive acceleration sensors ('tilt sensors') with have each two acceleration channels are mounted within the probe.

Although DLRs instrument with the heat flow probe was ready to launch in 2016 the time has been used to further improve the instrument. Dependent on the type of the probe, peak accelerations of about 200000 m/s² were measured at their housings. In case the accelerometers/tilt sensors encounter these loads a breakdown of the sensors is very likely, as their shock load limit is $a_{s,max} = \pm 34335\ \mathrm{m/s^2}$ (3500 g). To protect the sensors and to assure the needed accuracy in measuring the probes tilt, a shock isolation interface is integrated into the heat flow probe. This interface is described and analyzed within this paper. Measurements taken with the improved probe are additionally presented.

Vibration and shock isolation devices are generally applied, where sensitive equipment need protection from exterior vibrations and shocks. These elements can be passive as well as semi-active or fully active [2]. Active isolation interfaces are used when high performances are needed or when multiple excitation sources generate vibration at a payload [3], [4], [5].

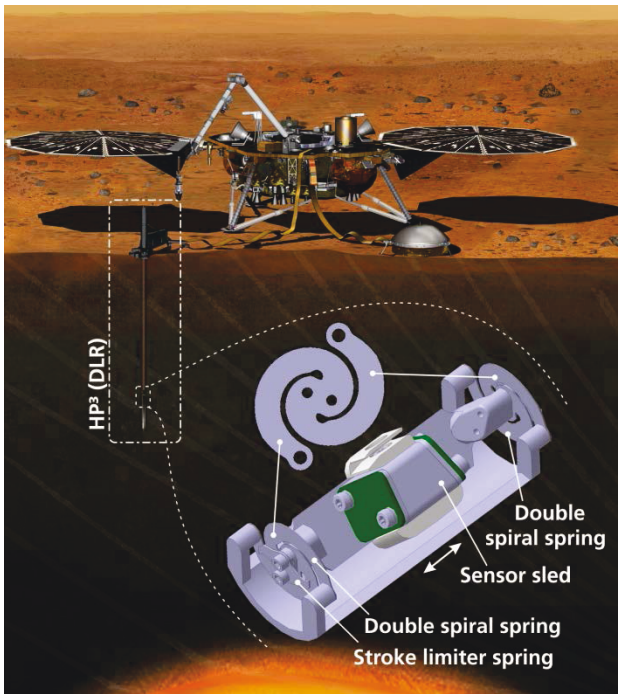

FIGURE 1. Artist's impression of the 'InSight' lander with the deployed HP³ instrument. Sensor sled with tilt sensors, shock isolation interface and launch protection system (STATIL) enlarged. Based on image from NASA/JPL-Caltech.

As in this particular system there is only minimal space and no electric supply for the isolation device provided, this paper focuses on passive isolation systems. An overview of this technique gives [6].

To reduce the peak acceleration at the resonance frequency of such isolation systems in the frequency domain, it is well known that an increasingly high damping

serves this task [7].

In contrast to that, the parameters of an isolation system have to be chosen differently to reduce the peak accelerations in the time domain, which is required to prevent the tilt sensors from getting damaged. How the optimal settings are calculated for such systems is expressed in the following section.

2. THEORETICAL BACKGROUND

Passive shock isolation systems are often modeled using a mechanical parallel arrangement of springs with the stiffness $k = 4 \cdot k_1$ and a dampers $d = 2 \cdot d_1$. Such systems connect a base system that is in this case the housing of the heat flow probe and a mass m. This mass m represents the structure that carries the accelerometers/tilt sensors. The base respectively the housing of the probe is accelerated with a_F and moves with the velocity v_F. The setup used within the probe of HP³ is indicated in the upper part of FIGURE 2, while the equivalent principle setup is indicated in the lower part.

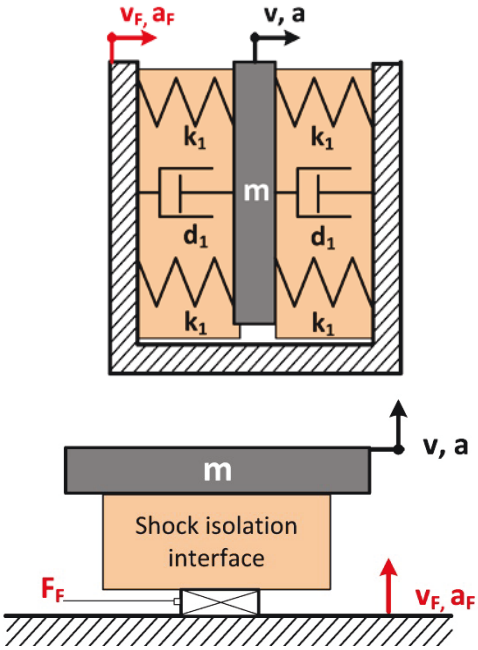

FIGURE 2. Used and principle setup of the shock isolation system within the probe of HP³.

Using such models, this section determines how the parameters of the isolation system should be chosen to minimize the peak accelerations.

The following calculations extend the information given in [8], where those aspects are more briefly described. They are based on mechanical impedances Z that are defined as the ratio between an exciting force F and a resulting velocity v. The impedance of a mass is therefore $\mathrm{Z_m} = \mathrm{s} \cdot \mathrm{m}$, for a stiffness it is $\mathrm{Z_k} = \frac{\mathrm{k}}{\mathrm{s}}$ and for a damper it is $Z_d = \mathrm{d}$, where s is equal to $j \cdot \omega$ with ω being the angular frequency. For compact writing the sum of the impedances $\mathrm{Z_k}$ and Z_d are substituted by $\mathrm{Z_{kd}}$, which is in this case the impedance of the shock isolation interface.

The impedance, that the system exhibits to the excitation v_F, is defined as $Z_F = F_F / v_F$. Using the model of FIGURE 2, it is found to be $\mathrm{Z_F} = \frac{\mathrm{Z_{kd}} \mathrm{Z_m}}{\mathrm{Z_{kd}} + \mathrm{Z_m}}$. The force F_F is then used to calculate the velocity $v = F_F / Z_m$.

The transfer function from the excitation v_F to the velocity v is consequently

$$(1) \qquad G(s) = \frac{Z_{kd}}{Z_{kd} + Z_m} = \frac{k + d \cdot s}{k + d \cdot s + m \cdot s^2}.$$

This equation can be separated into a stiffness dependent part $C(s)$, which ist the compliance and a damping depended part $Y(s)$, which corresponds to the admittance of the system:

$$(2) \qquad \begin{aligned} G(s) &= k \frac{1}{k + d \cdot s + m \cdot s^2} + d \frac{s}{k + d \cdot s + m \cdot s^2}, \\ &= k \cdot C(s) \; + \; d \cdot Y(s). \end{aligned}$$

The peak value of the magnitude of this equation is found at

$$(3) \qquad f_r = \frac{1}{2\pi} \sqrt{\frac{-k^2 m + \sqrt{k^3 m (2d^2 + km)}}{d^2 m}}$$

to be

$$(4) \qquad |G(s)|_{max} = \frac{\sqrt{k^2 + 4d^2 \mathrm{f_r}^2 \pi^2}}{\sqrt{4d^2 \mathrm{f_r}^2 \pi^2 + (k - 4\mathrm{f_r}^2 m \pi^2)^2}}.$$

With the inverse Laplace transforms of $C(s)$ and $Y(s)$ one finds the impulse response of the interface in the time domain:

$$(5) \qquad g(t) = k \cdot c(t) \; + \; d \cdot y(t).$$

Where $\mathrm{y(t)} := \frac{1}{\mathrm{m} \cdot \omega_\mathrm{d}} \mathrm{e}^{-\delta \cdot \mathrm{t}} \cdot (\omega_\mathrm{d} \cos(\omega_\mathrm{d} t) - \delta \sin(\omega_\mathrm{d} t))$ and $\mathrm{c(t)} := \frac{1}{\mathrm{m} \cdot \omega_\mathrm{d}} \mathrm{e}^{-\delta \cdot \mathrm{t}} \sin(\omega_\mathrm{d} t)$ are the indicated substitutes of EQUATION (5), in which δ equals $\frac{d}{2 \cdot m}$ and ω_d is equal to $\frac{\sqrt{4 \cdot \mathrm{k} \cdot \mathrm{m} - \mathrm{d}^2}}{2 \cdot \mathrm{m}}$.

The peak value of $g(t)$, which needs to be minimized to protect a structure from shocks, is found at

$$(6) \qquad \mathrm{t_1} = \frac{2m}{\sqrt{-d^2 + 4km}} \mathrm{ArcCos}\left[-\frac{d(d^2 - 3km)}{2k^{3/2} m^{3/2}} \right]$$

to be $\mathrm{g}(t)_{max} = \mathrm{g}(t_1)$:

$$(7) \qquad \mathrm{g}(t_1) = \frac{e^{-\frac{dt_1}{2m}} (d\omega \mathrm{dCos}(t_1 \omega_d) + (k - \frac{d^2}{2m}) \mathrm{Sin}(t_1 \omega_d))}{m \omega_d}.$$

The absolute values of the terms $G(s)$, $k \cdot C(s)$ and $d \cdot Y(s)$ in the frequency domain are presented in the upper parts of FIGURE 3 and FIGURE 4. In the lower parts are the impulse responses $g(t)$, $k \cdot c(t)$ and $d \cdot y(t)$

displayed. The figures are calculated for $k = 1065\,\mathrm{N/m}$, $m = 0.036\,\mathrm{kg}$ and $\mathrm{d} = 2\,\mathrm{kg/s}$ in FIGURE 3 and for $\mathrm{d} = 5\,\mathrm{kg/s}$ in FIGURE 4. It becomes obvious that the peak value of the impulse response is stiffness dominated in FIGURE 3 and dominated by the damping in FIGURE 4.

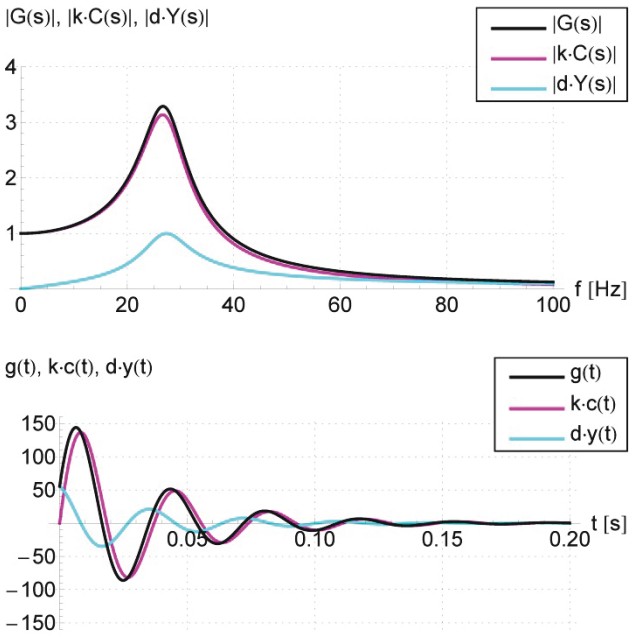

FIGURE 3. Frequency (top) and impulse response (bottom) of a shock isolation systems with the parameters of k=1065 N/m, m=0.036 kg and d=2 kg/s.

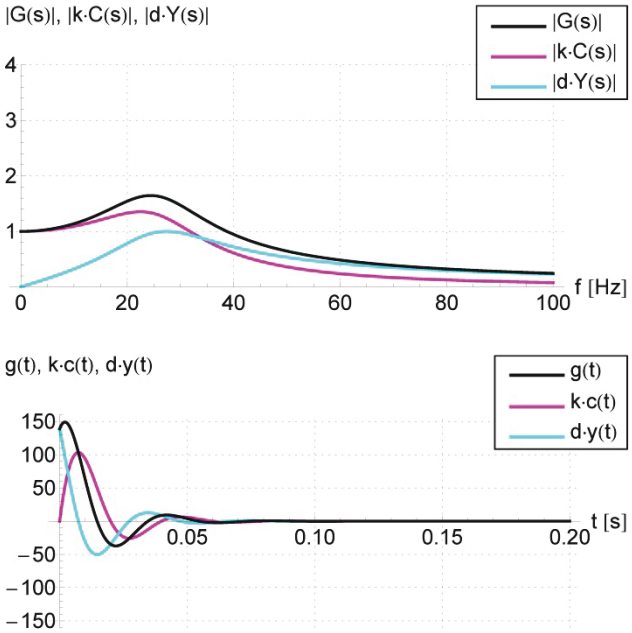

FIGURE 4. Frequency (top) and impulse response (bottom) of a shock isolation systems with the parameters k=1065 N/m, m=0.036 kg and d=5 kg/s.

FIGURE 5 compares the peak values in the frequency domain with the peak values of the impulse response of the system as function of the damping d. The previous parameters of the stiffness k and the mass m remain the same as for the calculation of the previous figures.

The peak level of the magnitude of the transfer function in the frequency domain (cf. EQUATION(4)) decreases asymptotically to $|\mathrm{G(s)}|_{max} = 1$ with increased damping d. If it is desired to reach a low frequency domain peak, system settings with high damping are beneficial; cf. black line in FIGURE (5). Nevertheless, as $|\mathrm{G(s)}|_{max} \approx 1{,}6$ at $d = 5$ a further increase of damping reduces the peak level only marginally. Furthermore, it shall be noted that setting a high damping results in a decreased isolation performance for high frequencies.

The red line of FIGURE (5) displays the maximum of the impulse response of the described isolation system, also as function of the damping d; cf. EQUATION (7). Different from the reduction of the peak in the frequency domain, a damping value that is for the described system lower than $6\,kg/s$ but larger than zero has to be set to reach a low maximum of the impulse response.

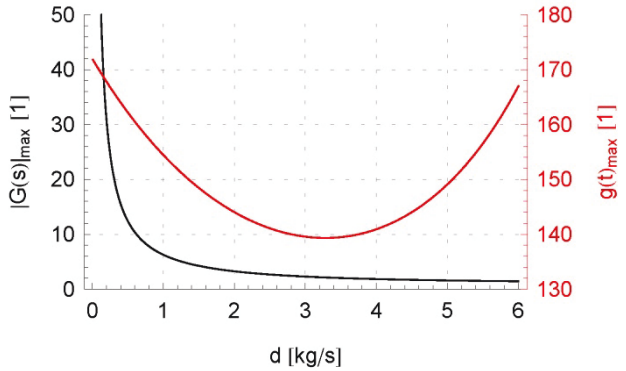

FIGURE 5. Peak values of the frequency response (black) and impulse response (red) of an isolation device with stiffness k=1065 N/m and mass m=0.036 kg as function of the damping d of the device.

For under-damped systems the optimal damping to achieve the lowest peak value in the time domain can be approximated by taking the stiffness k and the mass m into account. Using the following equation the optimal damping for the system of FIGURE 5 is calculated to be $d_{opt.} \cong 3.1\,kg/s.$ As indicated in [8], the EQUATION (8) holds true for a wide variety of system parameters.

$$\mathrm{d_{opt.}} \cong \frac{1}{2}\sqrt{\mathrm{k} \cdot \mathrm{m}}. \tag{8}$$

Expressed using the damping ratio β , which is defined as $\beta = \mathrm{d}/\left(2\sqrt{k \cdot m}\right)$, the approximated optimal value is

$$\beta_{opt.} \cong 0.25. \tag{9}$$

3. ISOLATION INTERFACE WITHIN THE PROBE OF HP³

A shock isolation interface is integrated into the probe of the HP³ system to protect the accelerometers/tilt sensors that are mounted on the green highlighted PCBs of FIGURE 1 from the shocks that occur during hammering.

Regarding this isolation system, only minimal changes have been implemented between the system described in [8], the system of the 2016 mission and the one that will fly in 2018. Nevertheless changes were made regarding other components inside the probe (e.g. the hammering mechanism). As the probe described in [8], was even a more previous development version than the one that was to fly 2016, new measurements are described in the following parts.

Nevertheless, the concept and the basic requirements of the isolation system within the heat flow probe of HP³ remain the same:

The shock isolation interface has to reduce the peak accelerations at the sensor sled in the direction, in that the soil is penetrated. As the hammering mechanism is guided inside the probe, this is the direction, in which high shock levels are present at the outer hull of the probe. The isolation interface has to have a low stiffness and roughly optimal damping in that direction (cf. SECTION 2 “theoretical background”).

As the probe hammers each 3 seconds, the mentioned tilt measurements have to be performed within this time frame. This clarifies the need to have an isolation interface which short decay time so that the sensor sled does not move while acceleration measurements (to calculate the systems tilt) are performed.

The sensor sled has to be precisely guided within the probe to enable the precise detection of the inclination of the system.

All these qualification requirements are fulfilled as the sled is supported by pairs of stacked double spiral (or 'galaxy') [9] springs at each side of the sensor sled (cf. FIGURE 1). The total number of used shock mitigation springs is four.

On the left as well as on the right (cf. FIGURE 1), these springs are mounted with bolts to the centered sensor sled. Each of the double spiral springs has a low stiffness along the axes of the sensor sled but has a much higher stiffness in the perpendicular directions.

Due to the centered sled, the pairs of double spiral springs are standing apart from each other. This prevents - in conjunction with the mentioned properties of the springs - the sled from being turned around any axes.

Damping – as calculated in SECTION 2 - can be added to this configuration with the addition of constrained layer damping foils. These foils can be integrated in-between a pair of double spiral springs or, if only one spring is used on each side, by adding the foils to the outside of one or both sides of the springs. This damping layers - either the ones in-between a pair of shock mitigation springs or the ones glued to their outside - are for terrestrial applications suitably made of elastomers with high damping properties.

In the described space application such damping layers cannot be added as the glass transition temperatures of those materials are usually higher than the temperatures that are expected to occur during cruise to planet Mars. Due to this boundary condition, damping is introduced into the system without damping layer foils but with friction that occurs in-between each pair of double spiral springs. Friction is caused during the movement of the sensor sled, as the arms of the pairs of double spiral springs to rub on top each other. Because the gradient of the red curve of FIGURE 5 is relatively low, it is sufficient to roughly reach the optimal value for the damping.

3.1. Isolation performance

The tilt sensors of the heat flow probe can precisely detect static acceleration of $\pm 16.7\ m/s^2$ $(\pm 1.7\ g)$ to perform measurements of the inclination of the mole within the ground. They are not suited to determine the peak acceleration (maximum shock levels) as the probe hammers into the soil because these loads are significantly higher.

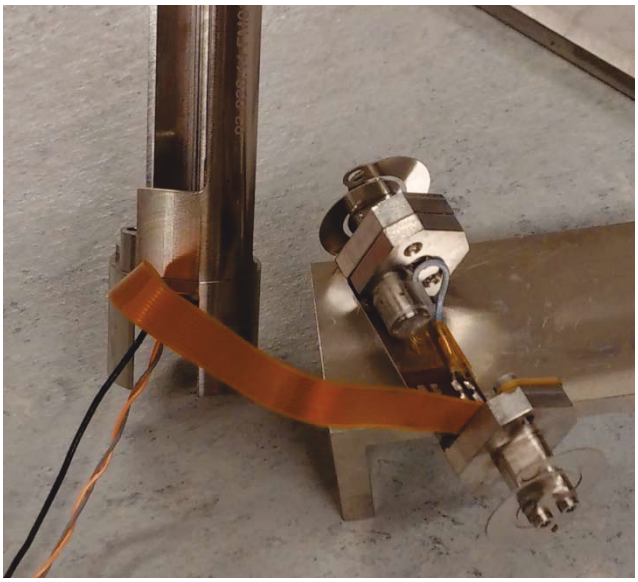

FIGURE 6. Modified sensor sled with an integrated dynamical acceleration sensor in-between the double spiral springs.

To evaluate the shock levels at the sled, the static accelerometers (tilt sensors) were replaced by a dynamical accelerometer with a measurement range of $49050\ m/s^2$ $(5000\ g)$. The signal of this sensor is fed though the very flexible ribbon cable that is indicated in FIGURE 6. The same cable is normally used for transmitting the tilt sensor signals. On one side it is mounted to the sensor sled and on the other to the housing of the probe. This cable induces only minimal stiffness between the housing and the sensor sled, which assures that the shock isolation interface remains even with this cable fully functional. The sensor lines of this cable are then fed though the top of the heat flow probe to the measuring device (black cable in FIGURE 7).

The effectiveness of the presented double spiral shock isolation interface was evaluated while the probe was hammering inside a sand filled basin (cf. FIGURE 7). The acceleration sensor (measurement range $\pm 490500\ \mathrm{m/s^2}$ or $\pm 50000\ \mathrm{g}$), with that the vibration of the housing are detected, is positioned on the top of the probe (sensor with blue cable).

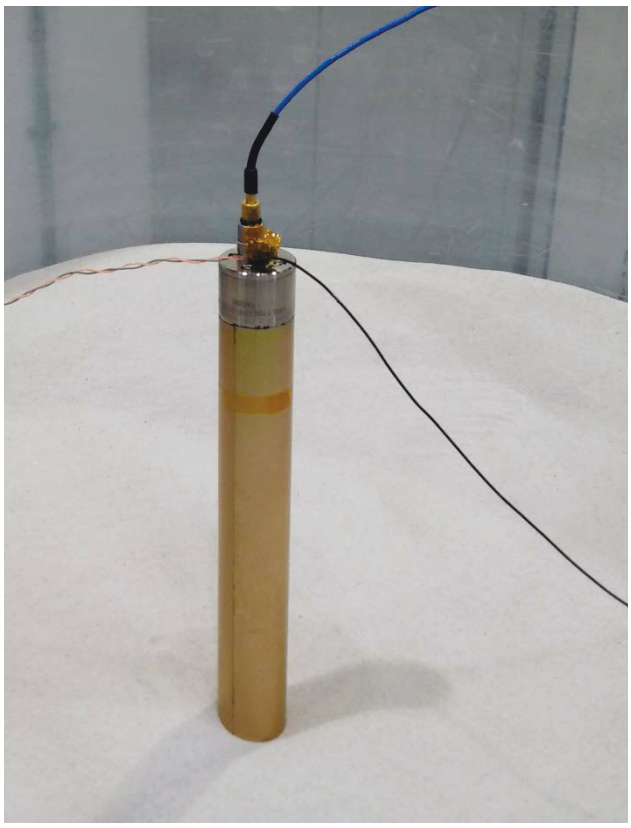

FIGURE 7. Heat flow probe with attached acceleration sensor on its top during a hammering test inside a sand filled basin.

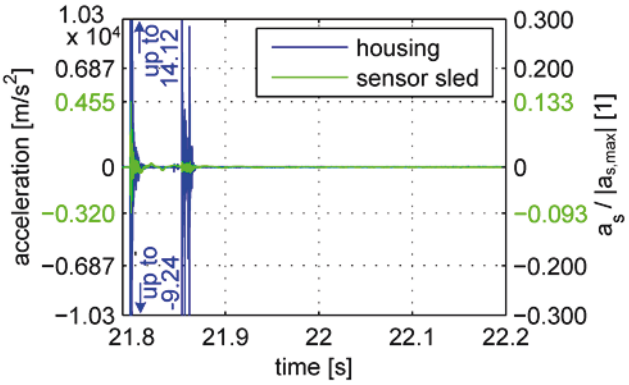

FIGURE 8. Comparison of accelerations at the housing of the heat flow probe (blue) and at the sensor sled in the interior of the probe (green), plotted over time.

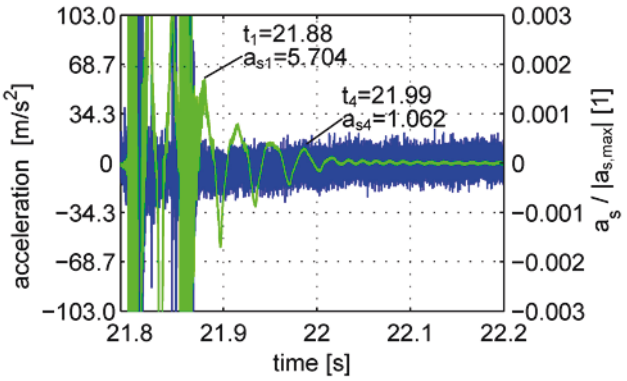

FIGURE 9. Zoom of FIGURE 10. Accelerations at the housing of the heat flow probe (blue) and at the sensor sled in the interior of the probe (green), plotted over time.

FIGURE 8 indicates the measured vibration of the housing in blue, while the green line indicates the interior vibration at the position, where the tilt sensors are usually integrated. The right axis indicates the ration of the measured accelerations and the shock load limit ($a_{s,max} = \pm 34335\ \mathrm{m/s^2}$) of the tilt sensors. The peak accelerations have been significantly reduced from 141166 m/s² (14390 g) at the outer housing to 4542 m/s² (463 g) at the sensor sled. The peak acceleration at the hull are 4.1 times larger than the shock limit of the tilt sensors, while the determined peak acceleration at the sensor sled is only 0.133 times their shock limit (less than 1/7th of their shock limit). This is equivalent to a reduction by a factor of $R_{is} = 31$. As the peak acceleration levels that the tilt sensors face are significantly lower than their shock limit (ratio $a_s/|a_{s,max}| \ll 1$) the sensors are effectively protected from the harmful shocks that occur during the hammering process (cf. FIGURE 8).

The overall shock levels at the housing of the probe changed compared to previous designs, were a similar isolation device reached a peak acceleration reduction of factor of $R_{is} = 127$ [8].

FIGURE 9 indicates a zoom of FIGURE 8. This figure is used to calculate the damping that is achieved by the actually implemented isolation system. As the blue signal is the output of the shock sensor with the measurement range of 490500 m/s² this line indicates mostly sensor noise in this highly zoomed figure.

The calculation of the damping is based on the on the decay constant (EQUATION (10)), which is determined using the period $T_d = \frac{t_n - t_1}{n-1}$ of the damped oscillation. The corresponding data points are highlighted in FIGURE 9. The number of the considered peaks is $n = 4$.

$$\delta = \frac{1}{(n-1)T_d} \cdot \mathrm{Log}\left[\frac{a_{s1}}{a_{sn}}\right] = 15.3\ \left[\frac{1}{s}\right] \quad (10)$$

From this value, the damping ratio β is calculated using the undamped Eigen frequency of the system:

$$f_0 = \sqrt{\left(\frac{1}{T_d}\right)^2 + \left(\frac{\delta}{2 * \pi}\right)^2} = 24.4\ \mathrm{Hz}, \quad (11)$$

$$\beta = \frac{\delta}{2 \cdot \pi \cdot f_0} = 0.09. \quad (12)$$

By taking the mass $m = 0.036\ \mathrm{kg}$ of the sensor sled into account, the stiffness $k = (2 \cdot \pi \cdot f_0)^2 \cdot m = 1065\ \mathrm{N/m}$ and the damping d can be calculated; cf. EQUATION (13).

$$d = 4 \cdot \pi \cdot \beta \cdot f_0 \cdot m = 1.1\ \mathrm{kg/s}. \quad (13)$$

Using this value and FIGURE 5, it is possible to determine the factor by that the peak reduction could have been increased, if the damping of the isolation system could have been set optimally.

For the realized damping of $d = 1.1\ \mathrm{kg/s}$ FIGURE 5 indicates a peak value of the impulse response of $g(t)_{max,is} = 153.1$. For the approximated optimal damping ($d_{opt} = 3.1\ \mathrm{kg/s}$) it indicates a peak value of $g(t)_{max,opt} = 139.4$. As the ratio of these values is $R_a = \frac{g(t)_{max,opt}}{g(t)_{max,is}} = 1.09$, it can be assumed that the peak reduction could be increased to $R_{opt} = R_{is} \cdot R_a = 33.8$ if the system were considered linear and the pulse being a Dirac delta.

Even though the realized damping is smaller than the approximated optimal damping (cf. SECTION 2), the system fulfills the given requirement for this application with significant margin.

FIGURE 10 indicates a longer recorded measurement of all four channels of the standard tilt sensors. These four signals are used to calculate the inclination of the probe within the ground. The signals were recorded during a thermal vacuum test of the device. To simulate Mars like environmental conditions the test was conducted within a CO_2 atmosphere, pressure being $8\ \mathrm{mbar}$ and temperature being $-55\ °C$. The figure indicates two full hammering cycles. As the tilt sensors are mounted on their sled in an inclined manner regarding the hammering vector, the accelerations are given in output voltages of the sensors.

After the start of a hammering cycle, the figure indicates only minimal oscillations of the sled in the simulated environmental conditions of planet Mars. The time frame in which the tilt measurements can be taken starts about 0.7 seconds after the first stroke of every hammering cycle.

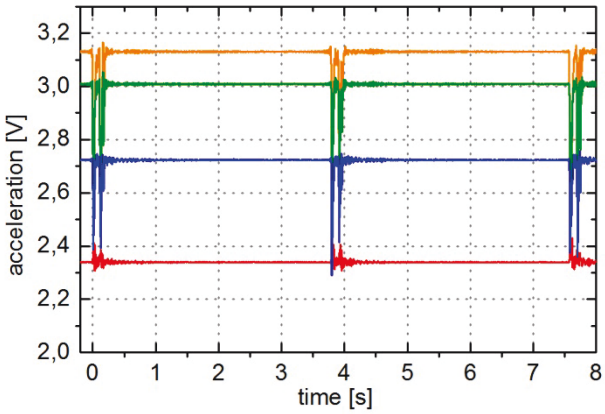

FIGURE 10. Accelerations at the tilt sensor caring sled over two cycles of the hammering process in the simulated Mars environment. All four tilt sensor channels (orange, green, blue, red) plotted over time.

3.2. Protection during launch and landing

The isolation system faces excessive loads during launch and landing. To prevent the double spiral springs from getting damaged due to overstretching in those mission phases, the maximum deflection of the sensor sled is limited by the surrounding housing. The maximum clearance, in that the sled is able to deflect, is limited to $\pm\ 2.9\ mm$ along the penetration direction of the probe.

When the sensor sled hits the deflection limiting walls, that are assumed to be infinitely stiff, it would be stopped almost instantaneously. This would cause excessive shock loads acting on the sensors. The occurrence of such shocks is prevented using the implemented shock isolation system as it is equipped with stroke limiter springs that are integrated to both sides of the sensor sled (cf. FIGURE 1). In case the sled is deflected these stroke limiter springs come into contact with the surrounding housing $0.3\ mm$ before the sled would hit the walls. This process decelerates the sensor sled gently, which prevents the occurrence of high shock loads during launch and landing. The corresponding stiffness plot of the pairs of double spiral springs in conjunction with the stroke limiter springs is indicated in FIGURE 11.

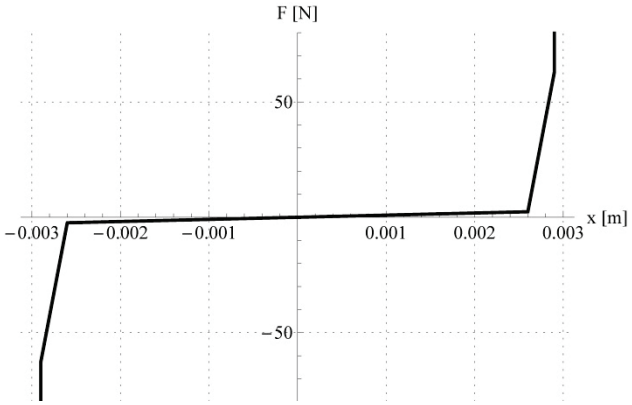

FIGURE 11. Reaction force of the shock isolation interface as function of deflection x of the sled.

Details on the analytical calculation of the occurring shock levels are presented in [8].

HP³ was excessively tested on a shaker system to qualify the instrument for launch. The induced vibrations result in the described a movement of the sensor sled along the axis of the probe.

The occurring peak accelerations were measured using the same modified sensor sled that is indicated in FIGURE 6. They were found to be about 1/7th of the shock load limit of the tilt sensors. FIGURE 12 displays the detected accelerations at the tilt sensors during the described shaker test and the acceleration ratio regarding the tilt sensors shock load limit.

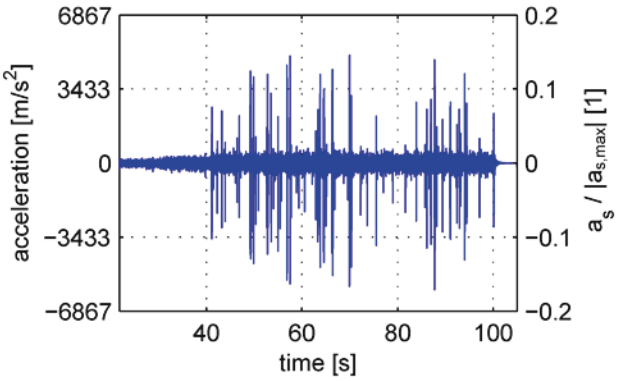

FIGURE 12. Time plot of the accelerations at the senor sled and the acceleration ratio regarding the shock load limit of the tilt sensors $a_s/|a_{s_{max}}|$. Measured during shaker tests to qualify the system for launch. Vibration levels ramped up to reach full levels at $t \approx 50\ s$.

4. SUMMARY AND CONCLUSION

Beginning with the description of the theoretical background for shock isolation devices, this paper clarifies how the optimal damping for such systems is calculated. Specifically, the shock isolation interface used to protect the sensitive accelerometers (tilt sensors) that are used inside the heat flow probe of the HP³ instrument, which is a part of the 'InSight' mission, is described in detail.

This interface is based on two pairs of flat double spiral springs (four springs in total), which mount the tilt sensor carrying sled to the housing of the probe. The required damping is generated with friction that occurs in-between the pairs of double spiral springs.

The peak accelerations at the sensor sled have been reduced to less than 1/7th of the maximum shock level that the tilt sensors can withstand. From comparing the accelerations measured at the housing of the probe and at the isolated sensor carrying sled, it was found that the transfer of the peak accelerations has been reduced by factor 31. The reduction factor depends on the design of the probe and the induced shocks. Using a different heat flow probe design with overall reduced shock levels and a similar shock isolation device, acceleration were reduced by factor 127.

Due to the directional dependent stiffness of the double spiral springs, the tilt sensors are not only isolated from the occurring shocks but in the same time precisely guided. This enables the accurate determination of the inclination of the heat flow probe within the Martian soil.

Furthermore, the integrated stroke limiters, which protect the double spiral springs and the tilt sensors during launch, are described. The stroke limiters decelerate the sled, on which the tilt sensors are mounted, as the whole system faces high loads during launch and landing.

It is shown, that the maximum peak accelerations that occur during the launch are significantly smaller than the shock level (about 1/7th of the limit) that the tilt sensors can withstand.

REFERENCES

[1] T. Spohn, M. Grott, S. Smrekar, C. Krause, and T. L. Hudson, "Measuring the Martian Heat Flow using the Heat Flow and Physical Properties Package (HP3)," in *45th Lunar Planet. Sience Conf.*, pp. 2–3 (2014).

[2] A. Preumont, *Vibration Control of Active Structures: An Introduction, 3rd Edition*, p. 432, Springer (2011).

[3] B. T. Kletz, J. Melcher, and M. Sinapius, "Active Vibration Isolation of Rear-View Mirrors Based on Piezoceramic Double Spiral'' Actuators," *Proc. of ISMA2012-USD2012*, 305–320, Leuven (2012).

[4] B. T. Kletz and J. Melcher, "Dual Feedback Control for Vibration Isolation Systems Dealing with Multiple Excitations," in *ICSV22*, Florence (2015).

[5] B. T. Kletz, *Aktive Schwingungsberuhigung mit reflektierenden und isolierenden Verbindungselementen in mehrfach angeregten Strukturen (Diss.)*, ISBN: 978-3-8440-5207-7, Shaker, Aachen (2017).

[6] E. I. Rivin, *Passive Vibration Isolation*, ASME (2003).

[7] D. Karnopp, "Active and semi-active vibration isolation," *J. Vib. Acoust.* **117**, 177–185 (1995).

[8] B. T. Kletz and J. Melcher, "Shock isolation on planet Mars," in *SSMET*, pp. 1–6, Braunschweig (2014).

[9] R. Lichtenheldt, "Hammering beneath the Surface of Mars : Analyse des Schlagzyklus und der äußeren Form des HP3-Mole mit Hilfe der Diskrete Elemente Methode," in *IFToMM D-A-CH*, Dortmund (2015).